Vertical growth rate of planted vegetation controls dune growth on a sandy beach

Strypsteen, Glenn; de Vries, Sierd; van Westen, Bart; Bonte, Dries; Homberger, Jan Markus; Hallin, Caroline; Rauwoens, Pieter

DOI
10.1016/j.coastaleng.2024.104624

Publication date
2024

Document Version
Final published version

Published in
Coastal Engineering

Coastal Engineering 194 (2024) 104624

Contents lists available at ScienceDirect

Coastal Engineering

journal homepage: www.elsevier.com/locate/coastaleng

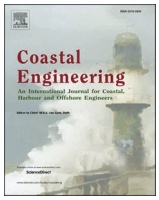

Vertical growth rate of planted vegetation controls dune growth on a sandy beach

Glenn Strypsteen [a,*], Sierd de Vries [b], Bart van Westen [b,c], Dries Bonte [d], Jan-Markus Homberger [e,f], Caroline Hallin [g], Pieter Rauwoens [a]

[a] Hydraulics and Geotechnics, Department of Civil Engineering, Bruges Campus, KU Leuven, Spoorwegstraat 12, 8200, Bruges, Belgium
[b] Delft University of Technology, Department of Civil Engineering and Geosciences, Stevinweg 1, Delft, 2628 CN, Netherlands
[c] Deltares, Boussinesqweg 1, Delft, 2629 HV, Netherlands
[d] Terrestrial Ecology Unit (TEREC), Department of Biology, Ghent University, Ghent, Belgium
[e] Plant Ecology and Nature Conservation Group, Wageningen University and Research, Wageningen, Netherlands
[f] Soil Physics and Land Management Group, Wageningen University and Research, Wageningen, Netherlands
[g] Faculty of Engineering, Lund University, John Ericssons väg 1, 223 63, Lund, Sweden

ARTICLE INFO

Keywords:
Dune development
Marram grass
Nature-based solution
Eco-morphodynamics
Aeolian sediment transport
AeoLiS

ABSTRACT

The integration of coastal dunes planted with vegetation and dikes combines traditional infrastructure with dynamic aeolian sediment and ecological processes to enhance coastal resilience. The functioning of such dune-dike hybrid Nature-based Solution strongly depends on aeolian sediment transport and the vertical growth rate of vegetation. We used the AeoLiS numerical model to investigate the relative importance of aeolian and vegetation dynamics in the evolution of a 120 m long and 20 m wide marram grass-planted dune field on a Belgian sandy beach backed by a seawall, constructed in 2021. AeoLiS proved to be a promising tool for predicting these systems, effectively capturing aeolian sediment deposition, vegetation growth, and profile development three years post-construction. Seasonal variations in vegetation trapping efficiency, driven by sediment burial, and seasonal plant growth emerged as important factors controlling dune growth. Profile development discrepancies were attributed to unaccounted biotic and abiotic factors, highlighting the complexity of coastal eco-geomorphological processes. Dunes planted with vegetation wider than 20 m were identified to enhance sediment trapping without an increase in dune height. These findings offer actionable insights for coastal management, promoting strategic dune design and planting approaches to reinforce shoreline resilience. Additionally, the findings underscore the necessity for advancing eco-morphodynamic models and deepening our knowledge of coastal dune dynamics.

1. Introduction

The European coastal regions are among the world's most densely inhabited areas. In many urbanized areas, natural sand dune barriers have been replaced by rigid coastal defence structures. Without the necessary measures to adapt, the number of people exposed to floods is anticipated to increase (Lomborg, 2020). Particularly in Europe, the coastal areas bordering the North Sea, Baltic Sea, and Atlantic Ocean face considerable flood risks due to rising sea levels. At the same time, climate extremes also threaten the Mediterranean coasts of Southern Europe (Vousdoukas et al., 2017).

The future of coastal management transcends the current paradigm of static flood defence structures. Hybrid Nature-based Solutions (NbS), which blend conventional hard infrastructure with dynamic sediment and ecological processes, are emerging as a promising approach (e.g., Derijckere et al., 2023; Strypsteen et al., 2024). These NbS are being developed along urbanized stretches of sandy European coasts, albeit on a limited scale (Derijckere et al., 2023; Elko et al., 2016; Matias et al., 2005; Stive et al., 2013; Strypsteen et al., 2024a; Tresca et al., 2014). Additionally, EU policies such as the Habitats Directive (The Habitats Directive - European Commission (europa.eu)) and Climate Change Adaptation Strategy (EU Adaptation Strategy - European Commission (europa.eu)) recognize the importance of dune conservation and management, further highlighting the role of dunes in coastal resilience and

* Corresponding author.
E-mail addresses: glenn.strypsteen@kuleuven.be (G. Strypsteen), bart.vanwesten@deltares.nl (B. van Westen), dries.bonte@ugent.be (D. Bonte), jan-markus.homberger@wur.nl (J.-M. Homberger), caroline.hallin@tvrl.lth.se (C. Hallin), pieter.rauwoens@kuleuven.be (P. Rauwoens).

https://doi.org/10.1016/j.coastaleng.2024.104624
Received 20 June 2024; Received in revised form 3 September 2024; Accepted 21 September 2024
Available online 24 September 2024

adaptation efforts. Notably, the integration of dikes and dunes into coastal protection strategies exemplifies this hybrid NbS approach, commonly referred to as dune-dike hybrid NbS (Bonte and Consortium, 2024). Such blue-grey infrastructure offers advantages in coastal safety and protection that neither rigid (dikes, seawalls) nor soft (beach nourishment, natural dunes) measures can achieve independently. These hybrid NbS function optimally only when both physical and ecological parameters are met, representing a fusion of engineering and ecological principles. This integrated approach indicates a new era in coastal management, underpinned by multidisciplinary collaboration and innovation.

In January 2021, a new artificial dune measuring 120 × 20 m^2 with marram grass (*Calamagrostis*-formerly *Ammophila-arenaria*) experimentally planted in six zones across the upper dry beach, was constructed along the Belgian coastline, at Oosteroever (Derijckere et al., 2023; Strypsteen et al., 2024a). Marram grass is a keystone species as it is burial tolerant, and its growth responses to burial, directly shaping the dune development (Bonte et al., 2021; Reijers et al., 2021). Marram grass traps aeolian sediment by reducing wind speeds near the bed (Keijsers et al., 2015; Raupach et al., 1993), and is resilient, sometimes being buried annually by more than 1 m (Strypsteen et al., 2024a; Bonte et al., 2021; Nolet et al., 2018; Wolfe and Nickling, 1993).

The intricate interplay between frequent aeolian sediment transport (Strypsteen, 2019; Strypsteen et al., 2019) and vegetation (Strypsteen et al., 2024a) is expected to drive the morphological evolution of the dune body, enhancing local coastal protection as shown by Derijckere et al. (2023) and Strypsteen (2023), which focused on the initial three and nine months following dune construction. Strypsteen et al. (2024a) found that the initial planting layout did not affect marram grass growth after three years of dune evolution. Adequate wind speed is necessary to initiate aeolian sand transport, particularly with an onshore and longshore component, leading to sand accumulation in the dune (Strypsteen, 2023). Factors like surface moisture and grainsize variability can limit sediment supply, affecting transport rates under different wind conditions and determining the maximum fetch length required for sediment saturation within the saltation layer (Strypsteen et al., 2024b).

State-of-the-art models for coastal aeolian sediment transport and dune development are able to simulate topographic development of coastal dunes and sediment transport at spatial scales relevant for coastal managers. An example is the process-based numerical AeoLiS model (de Vries et al., 2023; Hoonhout and de Vries, 2016). The extended version of AeoLiS, described in van Westen et al. (2024a), now integrates topographic steering impact on wind shear, steep slope avalanching, and vegetation dynamics, including growth and wind shear reduction. It accurately simulates sediment transport and morphological transformations driven by wind in coastal settings. Recent studies have showcased the model's ability to simulate various phenomena, including multi-fraction sediment transport (van IJzendoorn et al., 2023), surface moisture (Hallin et al., 2023), barchan and parabolic dunes (van Westen et al., 2019, 2024a), sediment trapping by vegetation (Dickey et al., 2023), and monthly artificial dune evolution (Strypsteen and de Vries, 2023). Although, the effect of different ecological conditions on longer term dune growth (i.e., years) has not yet been studied with AeoLiS, mainly due to a lack of high spatial and temporal data on dune growth and vegetation development.

AeoLiS integrates the primary processes driving dune growth in coastal areas but does not directly account for marine influences on beach and dune erosion. However, some studies have integrated an analytical dune erosion model, based on wave impact theory, into AeoLiS for one-dimensional cases (Heminway et al., 2024). It is noted that dunes can erode rapidly within hours during high storm surges and large waves, while growth due to aeolian processes is much slower during calm conditions (de Winter et al., 2015).

While aeolian sediment fluxes reaching the dunes are pivotal for understanding system development, the sediment accumulation along the dune profile and its interaction with vegetation profoundly influences the dune morphology (Durán and Moore, 2013). Although the relevance of dune-building grasses has been recognized (Hesp, 2002), most geomorphological studies have concentrated on the role of sand supply, determined by sand availability and wind-transport potential, in the dune-forming process (Bauer and Davidson-Arnott, 2003; Cohn et al., 2019; Delgado-Fernandez and Davidson-Arnott, 2011; Hesp, 1988; Hoonhout and de Vries, 2019; Psuty, 2004; Short and Hesp, 1982; van Westen et al., 2024b). This dynamic relationship between sediment fluxes and vegetation was highlighted by Heminway et al. (2024). They found that high-density, uniform planting strategies trap sediment near the dune toe, while low-density plantings may facilitate accretion across a wider area of the dune face. This finding aligns with the field observations of Derijckere et al. (2023) within the first three months following construction at the planted dune pilot site in Oosteroever, Belgium.

Our study aims to utilize AeoLiS to simulate the ecological and morphological characteristics of the planted dune pilot site in Oosteroever, Belgium. Our hypothesis is that dune evolution is directly related to changes in vegetation density. The objectives of this research are threefold: (1) to evaluate dune evolution under varying ecological growth conditions, (2) to calibrate AeoLiS using high-resolution field data obtained by Strypsteen et al. (2024a) for the dune site, and (3) to conduct a sensitivity analysis to gain insights into the behaviour of planted dune areas, with a focus on different dune widths plantations.

2. Materials and methods

2.1. Description of the experimental site

In January 2021, marram grass (*Calamagrostis arenaria*) was introduced to the upper beach of Oosteroever, Belgium situated approximately 2 km north of Ostend along the North Sea coast (Fig. 1). Backed by the "Spinoladijk" seawall and inland dunes, Oosteroever beach spans about 320 m in width, with sediments composed of medium to fine sand with a median grain size of 0.25 mm (Derijckere et al., 2023; Strypsteen, 2023). The gradual slope of the beach, with a ratio of 1:50 towards the dry beach, is combined with partially covered groins. The tide is semi-diurnal, with a tidal range of 3.5 m during neap tides to 5 m during spring tides. Tidal currents are in the order of 1–1.2 m/s (Haerens et al., 2012; Montreuil et al., 2016).

To study the impact of planting densities and patterns on dune development, marram grass was planted across six neighbouring zones, each measuring 20 × 20 m^2. These zones encompassed three densities (6, 9, and 15 plants/m^2) and four patterns: gridded, clustered, staggered, and random. Derijckere (2021) and Derijckere et al. (2023) examined the effects of these planting strategies on initial dune formation. Planted 0.15 m into the sand over two weeks, the marram grass had a protruding aboveground leave length of 0.35–0.45 m. Each planted tussock consisted of 5–7 leaves.

Enclosed by a steel-wire fence to restrict beach access and allow natural dune development, zone B (Fig. 1B) was positioned at +7.5 m TAW (Belgian Ordnance Datum, with MSL at +2.5 m), while the seawall crest is at +9.4 m TAW. Zones A, B, and C (Fig. 1B) are designated as areas free from management activities such as bulldozing. However, sand was relocated four times around these zones in the period between February 2021 and February 2024, from in front of the seawall toward the high-waterline. This relocating resulted in piles of sand of up to 2 m high (Strypsteen et al., 2024a). The artificial dune, placed seaward of the seawall (in zone B), employed a nature-based approach to enhance local coastal protection and mitigate sand nuisance. More details on the study area and pilot project can be found in Strypsteen et al. (2024a).

2.2. Numerical model description

AeoLiS is designed to simulate the complex spatio-temporal dynamics of aeolian sediment transport in supply-limited environments by

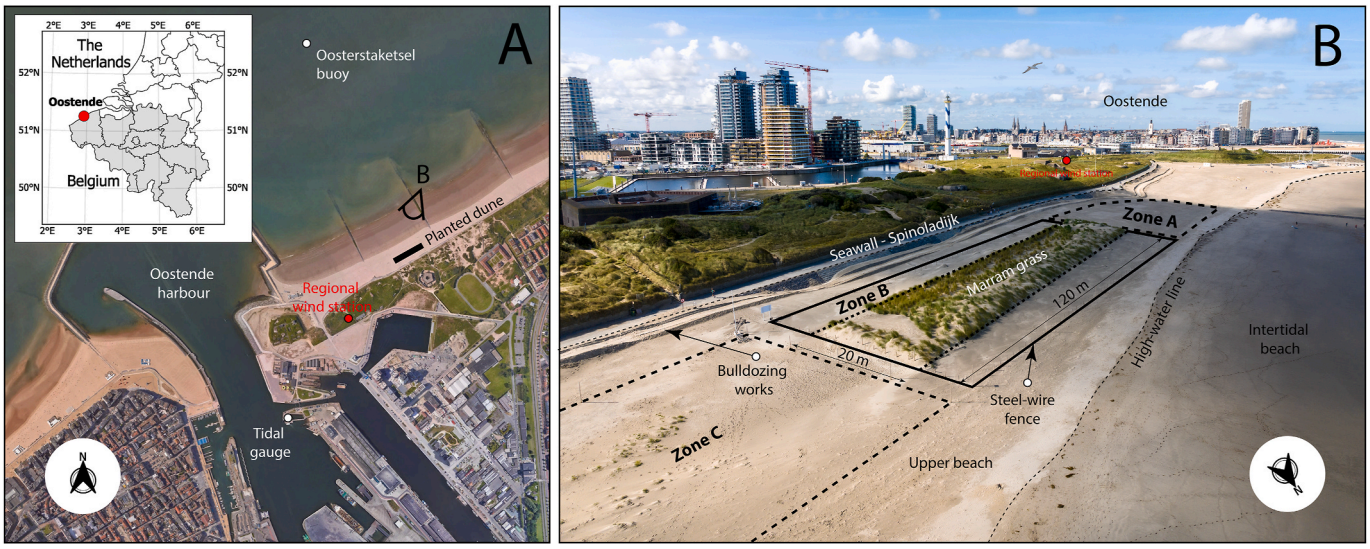

Fig. 1. A) Location of the planted dune east of the municipality of Oostende, Belgium. The location of the regional wave buoy, tidal gauge and wind station is shown. B) An aerial image (© Glenn Strypsteen) taken on August 8, 2023, offers an oblique perspective of the pilot project site, revealing key elements including project boundaries, the dune fence, marram grass, seawall, intertidal zone, and upper beach. The dune stretches alongshore for 120 m and spanning 20 m cross-shore. No bulldozer activities are allowed in Zones A, B, and C. Notably, Zone B is enclosed by a steel-wire fence.

discretization on a 2D depth-averaged grid (van Westen et al., 2024a; de Vries et al., 2023; Hoonhout and de Vries, 2016). In each model grid cell, local wind properties, including bed shear stress and wind velocity, are used to calculate sediment transport rates for individual grain size bins (d_n). As wind entrains and transports sediment via saltation, equilibrium sediment transport fluxes (q_p) are computed based on grain-related shear velocity using the bed roughness predictor and modified Bagnold transport equation of van Rijn and Strypsteen (2020):

$$q_p = \alpha_B \bullet \sqrt{\frac{d_{50}}{D}} \bullet \frac{\rho_{air}}{g} \bullet \left(u^3_{*,grain} - u^3_{*t}\right) \quad (1)$$

where ρ_{air} [kg/m^3] represents the air density, D [m] is a reference grain size of 0.25 mm, $u_{*,grain}$ [m/s] denotes the grain-related shear velocity based on a roughness predictor (not shown here, see Strypsteen (2023)), u_{*t} [m/s] is the threshold shear velocity below which transport does not occur, and α_B [−] is an empirical coefficient. The shear velocity threshold for transport is calculated using the Bagnold equation (Bagnold, 1954).

In AeoLiS, the influence of vegetation on dune evolution is comprehensively addressed. This includes modelling the intrinsic growth of vegetation, accounting for factors such as growth and decay due to burial (Durán and Moore, 2013), lateral expansion and establishment (Keijsers et al., 2016), as well as simulating the destruction of vegetation caused by hydrodynamic processes. In the event of cell inundation, vegetation density is set to zero as a result. Inspired by the Coastal Dune Model (CDM) proposed by Durán and Moore (2013), AeoLiS incorporates vegetation-wind interaction using the expression established by Durán and Herrmann, 2006a,b.

$$\frac{u_{*veg}}{u_*} = \frac{1}{\sqrt{1 + \Gamma \rho_{veg}}} \quad (2)$$

where the ratio of shear velocity in the presence of vegetation ($u_{*,veg}$) to the unobstructed shear velocity (u_*) is determined by a vegetation-related roughness parameter (Γ) and the vegetation density within a unit area of the grid cell (ρ_{veg}). In the model, $\Gamma = 16$ is derived from plant form drag and geometry values documented for creosote communities (Durán and Herrmann, 2006a,b). At the pilot site, the vegetation consists solely of marram grass, forming a monoculture. The same value for marram grass was applied due to its similarity in size. Theoretically, Γ is expected to vary across growing seasons due to changes in the plant's geometry and the influence of neighbouring plants, which can alter the plant's shape through sheltering effects. However, Γ is kept constant throughout the simulations. This implementation calculates the expression on each model grid cell, with higher vegetation density (expressed by ρ_{veg}) leading to a more substantial reduction in shear velocity compared to sparse vegetation (Fig. 2B). By integrating these physical and ecological processes, AeoLiS simulates spatial patterns and temporal variations in sediment transport and morphological changes resulting from aeolian processes in coastal environments.

The density, ρ_{veg}, can vary in space and time and is determined by the ratio of the actual vegetation height (h_{veg}) to the maximum vegetation height ($h_{veg,max}$), and can vary between 0 and 1 (Durán and Herrmann, 2006a,b):

$$\rho_{veg} = \left(\frac{h_{veg}}{h_{veg,max}}\right)^2 \quad (3)$$

This assumption is based on the idea that burying vegetation reduces its height, which indicates a decrease in actual cover. For marram grass, this holds true since its highest biomass density is near the surface, with a substantial decrease as height increases. While this may apply to a single tussock, it becomes less accurate when assessing the frontal surface area and density of vegetation as more plants grow and cover the area. In the model, $h_{veg,max} = 1$ m, a value supported by ground-truthing observations conducted by Strypsteen et al. (2024a).

The change in vegetation density per grid cell is directly linked to the alteration in vegetation height within that specific cell. This height variation is influenced by both the growth rate of the vegetation and the rate of sediment burial. If the vegetation density remains constant over time, it suggests either no sedimentation or a growth rate equal to the rate of sediment burial within the cell. Vegetation growth and decay follow the model proposed by Durán and Herrmann (2006a), (2006b) modified to include $\delta z_{b,opt}$ (m/year), representing sediment burial for optimal growth that shifts the peak of optimal growth (Fig. 2A):

$$\frac{\delta h_{veg}}{\delta t} = V_{ver}\left(1 - \frac{h_{veg}}{h_{veg,max}}\right) - \gamma_{veg}\left|\frac{\delta z_{b,veg}}{\delta t} - \delta z_{b,opt}\right| \quad (4)$$

Here, γ_{veg} (default = 1) is a sediment burial factor that accounts for the impact of sediment burial on vegetation. The height of the vegetation (h_{veg} in m) cannot be less than zero. V_{ver} represents the maximum

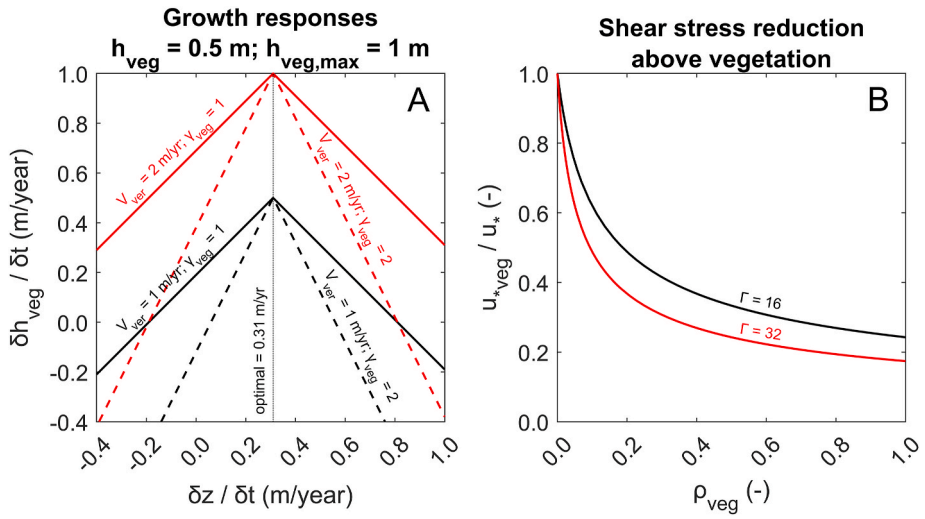

Fig. 2. A) The vegetation growth response varies with different vertical growth rates (example for V_{ver} = 1 and 2 m/year). Optimal vegetation growth is determined by a burial rate of 0.31 m/year, with a maximum vegetation height set at 1 m and a plant height of 0.5 m. Additionally, the growth response for varying burial factors is depicted (λ_{veg} = 1 and 2). B) Shear stress reduction for two different vegetation-related roughness parameters and vegetation densities (Γ = 16 and 32).

vertical growth rate of vegetation given in m/year, while the sediment burial rate $\delta z_{b,veg}$ [m] is determined as the bed level change per time step. By simply converting this value to a bed level change per year multiple errors are induced, as the time scale over which the bed level change actually occurs is much shorter than this one year. To compare the bed level change per time step with the vegetation growth rate per year, an average bed level change is estimated over a specified time (default is one day). This average is then extrapolated to an annual rate and applied in Eq. (4). This method ensures that sudden changes in the bed level change over one time step are not used as an estimate of the total bed level change in one year, which would be far too high.

The optimal growth rate for certain vegetation species in dune environments is depending upon sediment burial (Maun, 1998). The optimal burial rate for maximum vegetation growth for marram grass for the neighbouring Dutch coast is around 0.31 m/year with a burying tolerance of 0.78–0.96 m burial/year (Nolet et al., 2018). This optimal value is used in the model. The relationship between sediment burial and vegetation growth for different vertical growth rates and burial factors is shown in Fig. 2A. V_{ver} contains information of meteorological and local conditions that enhance or inhibit vegetation growth process (Danin, 1991; Hesp, 1991). Furthermore, vegetation growth is very slow in the winter but does not stop entirely (Huiskes, 1979). V_{ver} in the model is varied between 0 and 6 m/year.

It is important to distinguish between the terms "vegetation density" and "vegetation cover," which are commonly used in discussions about vegetation. "Vegetation cover" refers to the percentage of a ground area covered by vegetation. In contrast, "vegetation density," also referred to as "lateral cover" as described by Marshall (1971) and Raupach (1992), pertains to the concept of shear stress partitioning above vegetation and defines the frontal area per unit ground area. In this study, we describe vegetation in terms of vegetation density rather than cover, as we utilize the partitioning method of Raupach et al. (1993) and Durán and Herrmann (2006a), (2006b) described in Eq. (2).

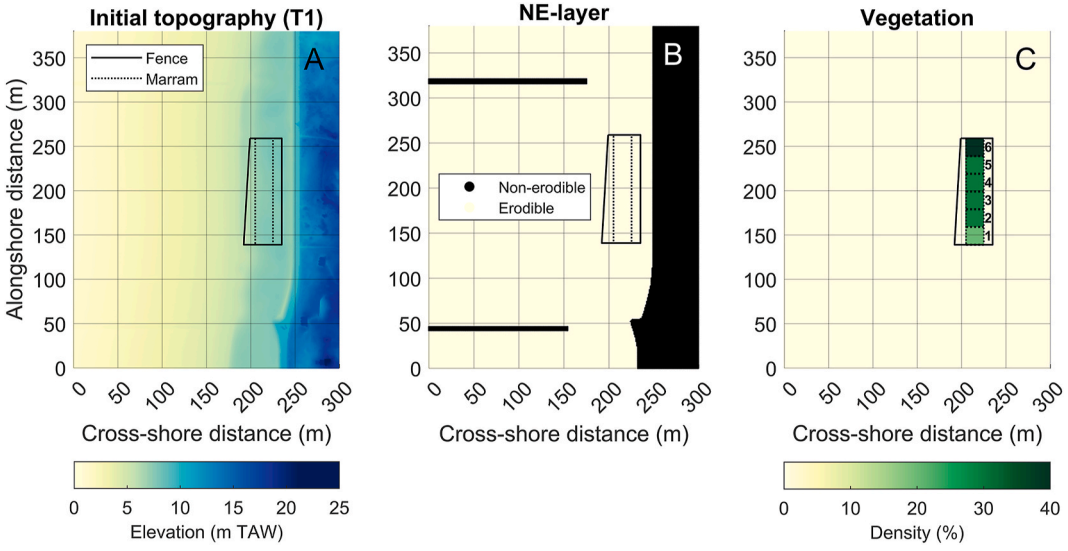

Fig. 3. A) 1 m-gridded model topography based on the T1 drone survey of March 2, 2021. B) Mask used to indicate the location of the erodible and non-erodible layer. Sediment below the non-erodible layer cannot be transported. C) Vegetation density used in the model to represent the presence of vegetation in the dune area. The six original planted zones are indicated by bold numbers. The fence around the dune area is shown with the black solid line.

2.3. Model grid and input parameters

The model's initial topography is rotated 29.4° relative to the dune toe orientation and interpolated on a 1 × 1 m^2 grid to conform with the AeoLiS grid input, with the x-axis representing the cross-shore distance and the y-axis the alongshore distance. This topography is derived from the drone survey conducted after planting the marram grass on March 2, 2021 (T1), covering an area of 380 m alongshore and 300 m cross-shore (Fig. 3A). To address the presence of groins and the seawall at the study site, a non-erodible layer mask is applied, ensuring that sediment erosion does not occur below initial topography. This mask extends to include the landward dunes (Fig. 3B). Additionally, the model incorporates three constant dune vegetation densities: 20%, 30%, and 40% (Fig. 3C).

Three years of regional hourly wind speed and direction data, measured at 10 m above the surface, was obtained from Meteopark Oostende (www.meetnetvlaamsebanken.be) (Fig. 4A and B). The regional station is located 325 m from the study site (2°55′48"E−51°14′15"N), positioned in the landward dunes (Fig. 1A). It also monitors meteorological parameters, including precipitation. The wind speed is transformed following Strypsteen (2023) to replicate beach conditions and is based on nine months of local wind measurements. Throughout this paper, three time periods of approximately one year each are defined based on 28 conducted drone surveys (indicated as T) as follows: Year 1 spans from February 12, 2021 to January 17, 2022 (T10); Year 2 extends from January 17, 2022 (T10) to January 24, 2023 (T20); and Year 3 covers the period from January 24, 2023 (T20) to February 27, 2024 (T28) (Fig. 4A).

Hourly offshore water levels, wave heights, and wave periods (Fig. 4C and D) are obtained from the nearby buoy Oostende Oosterstaketsel and Oostende harbour (Fig. 1A) and are imposed to the model as well. Four storms, with significant wave heights above 3.5 m, impacted the study site where wave runup approached the dune toe: Storm Corrie (January 31, 2022), Diego (April 01, 2022), Larisa (March 10, 2023), and Ciaran (November 24, 2023). Storm Corrie caused minor dune toe erosion, as indicated by Strypsteen et al. (2024a). The wind climate follows a seasonal pattern (Fig. 4E) with peak wind speeds typically accompanying winter storms. Additionally, marine conditions fluctuate seasonally following the wind climate (Fig. 4F and G), with the lowest wave energy and water levels typically observed during summer. In contrast, winter experiences larger waves.

A single grain size fraction, with the measured median grain size, is set to 0.25 mm to reduce computational time (Strypsteen, 2023). A single grain size fraction typically produces similar simulated results to multi-fraction simulations on timescales ranging from days to years (van IJzendoorn et al., 2023). Only the important processes are enabled and refer to wind, wind shear, tide, runup, waves, threshold, sediment transport, separation bubble, vegetation and bed update. No additional tuning of model parameters was undertaken, except for the empirical coefficient (α_B) in van Rijn and Strypsteen (2020) is set to 1.5 instead of 2. Using AeoLiS v3 (de Vries et al., 2023), computational times were approximately 3 h (on a HP ZBook with 11th Gen Intel(R) Core(TM)

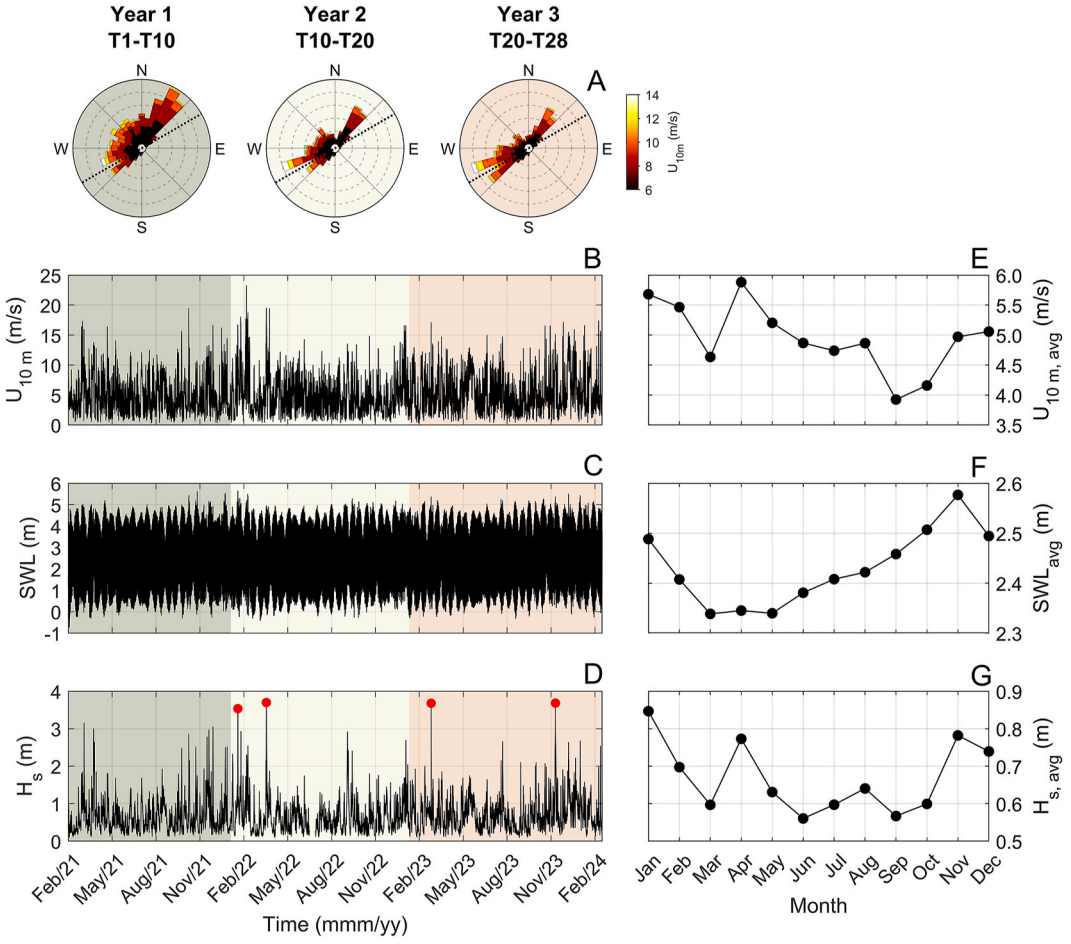

Fig. 4. A) Wind roses for three consecutive annual time periods. B) Three years timeseries of transformed local wind speed, C) still water levels, and D) wave height. The wind measurements are obtained from Meteopark Oostende. The hydrodynamic measurements are obtained from Oostende Oosterstaketsel wave buoy and Oostende harbour (Fig. 1). The red dots indicate the four events where wave runup approached the dune toe. From left to right: storm Corrie (January 31, 2022), Diego (April 01, 2022), Larisa (March 10, 2023), Ciaran (November 24, 2023). E-G) Monthly averages of local wind speed, still water levels, and wave height.

i7-11800H @ 2.30 GHz processor).

2.4. Modelling and calibration approach

A two-dimensional model is setup for the case study. Circular conditions are used on the lateral boundaries, meaning when sediment exits one side it re-enters from the opposite side. The model is calibrated using three years of comprehensive field data covering wind, tides, waves, vegetation, and topography. These conditions are described in detail by Strypsteen et al. (2024a). Throughout the period between February 12, 2021 and February 27, 2024, the magnitudes and patterns in volumetric dune and beach changes, dune height, and profile changes are simulated. The start of this period is two weeks after the marram grass was planted.

Initially, the calibration focused on the first nine months following dune construction, during which the dune was 100% effective in trapping sediment. In this phase, vegetation vertical growth was set to a high level (i.e., 6 m/year) to ensure that vegetation density would be sufficient to trap all sediment originating from the beach. This initial calibration was already conducted by Strypsteen and de Vries (2023). Next, different but temporally constant vertical growth rates for vegetation is explored, ranging from 0.5 to 6 m/year, to understand their impact on dune volume and profile changes for the entire study period. Consequently, the calibration process shifted to account for dynamic ecological processes as shown in Fig. 5. This involved adjusting the vegetation vertical growth rate and maximum height over time to account for seasonal variability and precipitation dynamics, which has previously not been done in AeoLiS. A callback function is implemented in AeoLiS to account for this temporal variability in vegetation dynamics. Specifically, higher growth rates were applied during the vegetation growing season and periods of increased precipitation. These adjustments were primarily conducted through trial and error.

The average precipitation at the Belgian coast is approximately 670 mm/year (Dauwe et al., 2019), highlighting that precipitation during the first two years of dune evolution was notably below average (Fig. 6), while the last months of the third year exceeded the average precipitation. These deviations, coupled with sediment burial rates and the vegetation growing season, likely influenced the vertical growth rate of vegetation. Growth during the growing season was likely subdued during the drier initial years but intensified during the third, wetter year. Homberger et al. (2024) observed that soil moisture levels in the upper 0.5 m beneath the surface closely follow precipitation patterns. Soil moisture plays a significant role in plant growth, with prolonged deviations from average growing season precipitation leading to notable impacts on vegetation growth: extremely dry years can reduce marram grass growth by up to 23%, while extremely wet years can increase it by up to 32% (Homberger et al., 2024).

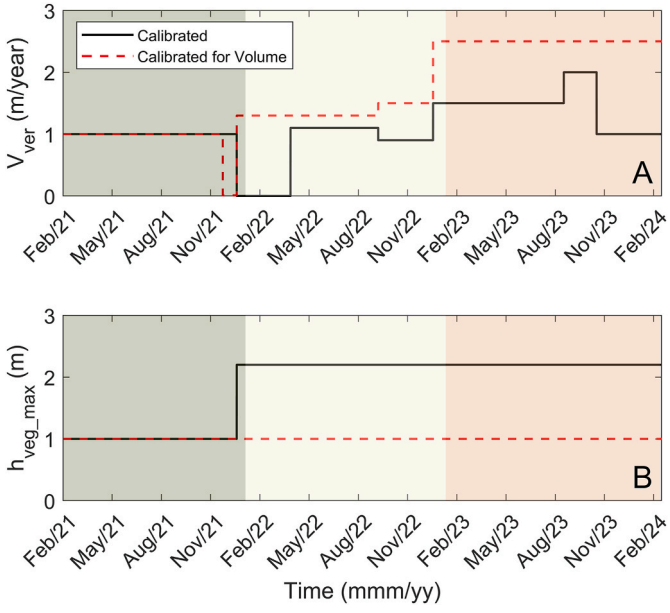

Fig. 5. A) Temporal variability in vertical vegetation growth rate for the calibrated model and the model calibrated solely for dune volume. B) Temporal variability in maximum vegetation height for the two calibrated models. The background colours represent the three years.

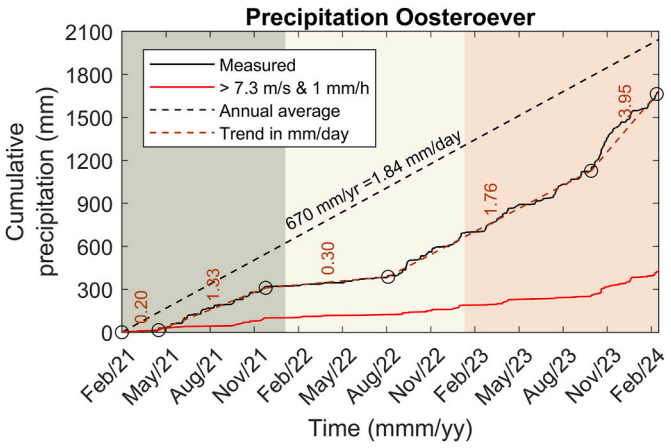

Fig. 6. Cumulative precipitation measured at the regional weather station. The solid red line indicates the cumulative precipitation for wind speeds higher than the threshold for aeolian sediment transport. The background colours represent the three years.

The three-year calibrated model is then used to explore different constructed dune widths, while maintaining consistent beach characteristics and water level fluctuations.

2.5. Post-processing

During the AeoLiS model simulations, data were stored in a netCDF file every one day, encompassing three years for each model run. Post-processing encompassed multiple steps: (1) assessing dune volume change, (2) comparing post-model mean dune profiles and dune crest level with observed data, (3) comparing beach volume change with observations, and (4) analysing the effects of different dune widths on profile development, mean dune crest level, and dune volume change starting from the calibrated model. The r^2-value and root-mean-square error (RMSE) are also calculated for the calibrated model following:

$$r^2 = 1 - \frac{\sum_n \left(V^n_{observed} - V^n_{simulated}\right)^2}{\sum_n \left(V^n_{observed} - \overline{V^n_{observed}}\right)^2} \quad (5)$$

$$RMSE = \sqrt{\sum_n \left(V^n_{observed} - V^n_{simulated}\right)^2} \quad (6)$$

with V = volume. The r^2-value and RMSE calculated for the first nine months of dune evolution by Strypsteen (2023) is 0.979 and 0.64 m^3/m, respectively.

Moran's index (I) is used to assess spatial autocorrelation between vegetation density:

$$\text{Moran's } I = \frac{n\sum_{i=1}^{n}\sum_{j=1}^{n} w_{ij}\left(x_i - \bar{x}\right)\left(x_j - \bar{x}\right)}{\sum_{i=1}^{n}\sum_{j=1}^{n} w_{ij}\left(x_i - \bar{x}\right)^2} \quad (7)$$

where w_{ij} is the spatial weight matrix; x_i and x_j are the vegetation density values at the ith and jth sampling points, respectively; n is the total number of samples; and $\bar{x}$ is the average value of the variable x. The Moran's I value ranges from −1 to 1. Specifically, Moran's I > 0 indicates a clustered spatial distribution of vegetation density values,

Moran's I < 0 signifies a dispersed spatial distribution, and Moran's I = 0 represents a random spatial distribution (Wang et al., 2021).

3. Results

In the results section, the deposition and erosion patterns of simulated and measured results (4.1), the effect of vegetation growth rates on dune volume changes (4.2), the simulated vegetation development (4.3), and the impact of vegetation growth rates on profile development (4.4), are detailed. Furthermore, dune development concerning different dune widths is analysed (4.5).

3.1. Deposition and erosion patterns for calibrated model

Patterns of deposition and erosion are shown in Fig. 7, where the comparison between the simulated topography changes and the measured topography changes is made. The model results demonstrate a reasonable accuracy in representing the distribution of sand within the planted dune area over the years ($r^2 = 0.992$ and RMSE = 0.68 m^3/m).

Initially, in the first year, sand distribution appears relatively uniform across the vegetation area, consistent with both model and measured results. However, in the second year, while dune growth is relatively small, there is a noticeable increase in measured sand deposition at the seaward and southwest boundaries, which is not reflected in the model results. By the third and final year, vegetation on the seaward side of the dune effectively traps more sediment, leading to a broader deposition area from the northeast towards the southwest. This trend is reflected in the measured results but not in the model results. However, similar but more pronounced to the second year, the model simulates a landward shift of the dune body, which is not observed in the measurements. Overall, despite differences between measurements and model results in detailed topography patterns across small spatial scales within the vegetation, the model effectively captures dune development across the relevant spatial-temporal scales.

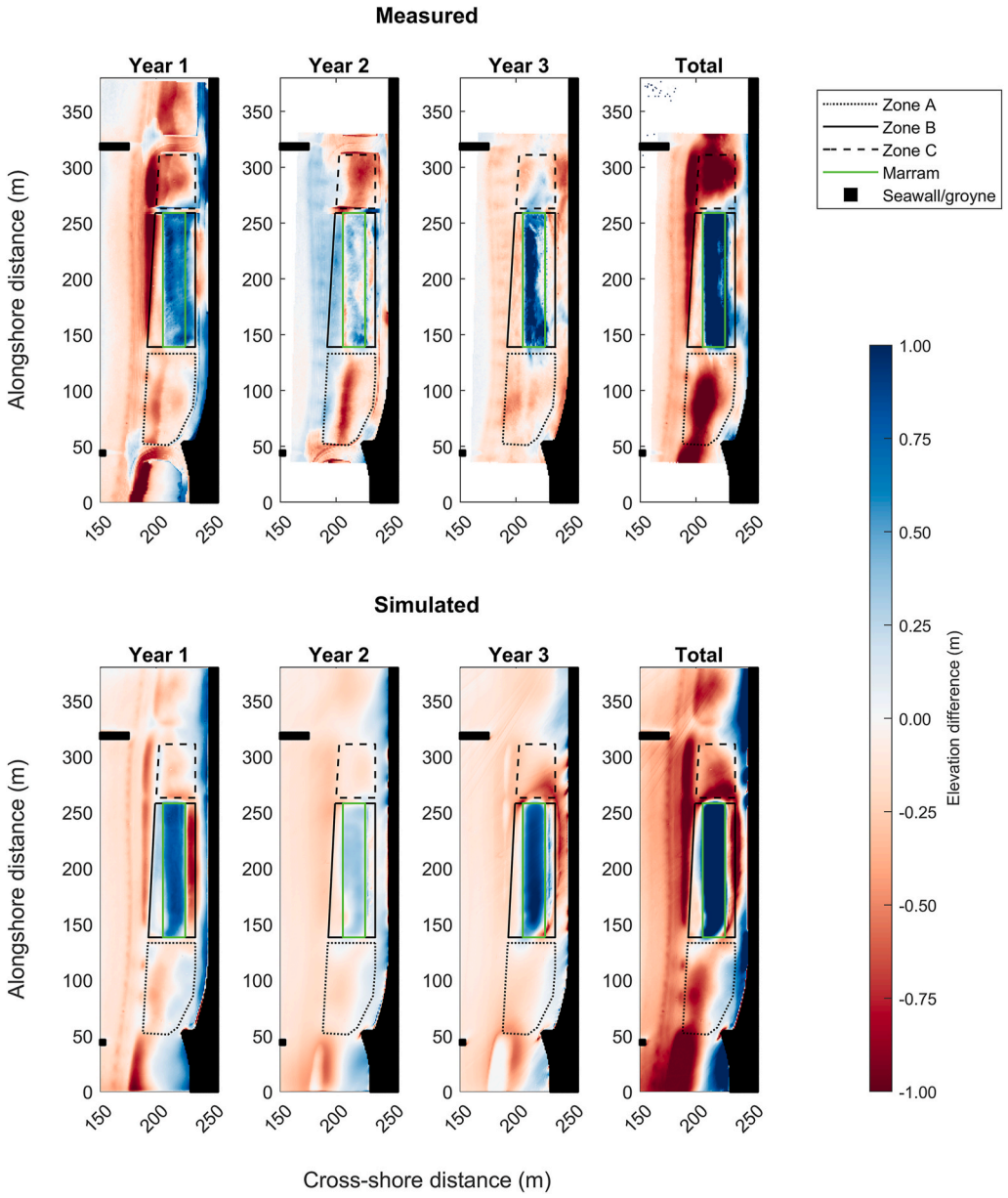

Fig. 7. Yearly deposition and erosion as measured and simulated, along with the corresponding differences. The model results solely account for aeolian sediment transport, as hydrodynamic sediment transport is not implemented in AeoLiS. Boundaries delineating zones A, B, C, and the marram grass area are denoted by dashed, dotted, and solid lines, respectively, and are free from bulldozing activities.

The measured erosion in the beach area around the planted dune exceeds the simulated erosion (Fig. 8) as sediment transport by marine processes are not considered in the AeoLiS simulations. Also notable is the higher erosion measured compared to the simulation at the beginning of the second year, attributed to storm Corrie on January 31, 2022, which caused significant beach erosion of 10–15 m^3/m and some dune erosion of 1.5 m^3/m due to wave processes and wind (Fig. 8). Additionally, in the second year, more sand accumulation occurred in the intertidal beach in the measurements than in the simulation. This difference is mainly attributed to bulldozing activities following storms Corrie and Diego, during which sand in front of the seawall was relocated to the high-waterline. This sand naturally redistributed by wind in the subsequent months of the second year. In the model, management activities are not simulated.

In the last year, measured beach erosion roughly follows the simulated trend (Fig. 8), particularly evident in zone A, with higher erosion observed in zone C compared to zone A, consistent with both measurements and simulations. The model predicts more erosion in zone C during the last quarter of the third year than was actually measured (Fig. 8), which is attributed to winds from the southwest. This discrepancy is linked to the abrupt increase in wind shear velocity when transitioning from the vegetated area to the bare sand surface (Strypsteen and de Vries, 2023). This effect is also evident in Fig. 7, between the landward boundary of the vegetation and the seawall.

3.2. Effect of vegetation growth rates on dune volume changes

Fig. 9A shows the changes in simulated dune volume to various vegetation growth responses. When the temporal constant vertical vegetation growth exceeds 1 m/year (with a maximum vegetation height of 1 m), simulated dune volume change closely matches measurements in the initial nine months until the end of October 2021, consistent with findings from Strypsteen (2023). Vegetation growth (Fig. 9C) and density can effectively keep up with sediment burial, resulting in 100% trapping of aeolian sediment by the vegetation (Fig. 9D). However, discrepancies between simulations with the different vegetation growth rates and measurements arise in subsequent months.

When a large vegetation growth rate is assumed in the model (V_{ver} = 6 m/year), vegetation keeps pace with sediment burial and exhibits an overall increase in density. Therefore an overestimation of dune volume change compared to measured values emerges. As shown in Fig. 9A, maximum dune growth would have reached 71.9 m^3/m after three years of wind forcing, marking a 227% overestimation compared to the measured volume of 31.7 m^3/m. Fig. 9B also illustrates that the beach contributes a high sediment input throughout the years, of which only a fraction is effectively trapped by the vegetation. These annual maximum accumulated transports at the dune toe correspond to the annual volume changes for maximum dune growth depicted in Fig. 9A.

A smaller constant vertical vegetation growth rate of 2 m/year also overestimates measured dune volume change in the second and third years. However, a decrease in dune growth occurs as a result of a significant decrease in vegetation density. Spatial variations in shear stress, influenced by topographic steering of the wind field, are responsible for this decrease in dune volume. Assuming a dune growth rate of 1 m/year leads to comparable dune volume changes between the model and measurements in the second year. However, a decrease in dune volume in the third year is simulated due to insufficient vegetation density causing spatial variations in shear stress. The deviating results between the model and measurements when assuming different but temporal constant vegetation vertical growth rates suggest that a variable vertical growth rate of vegetation with time may be necessary to improve the results of the simulation.

The discrepancy between the different simulations and measurements becomes apparent when the average simulated vegetation density (ρ_{veg}) falls below 5% (Fig. 9C). In this scenario, not all aeolian sediment can be trapped, resulting in sediment bypassing the dune. When burial rates fall below or exceed the optimum value of 0.31 m/year, a decline in vegetation growth becomes evident (Fig. 2A). During the period from November 2021 to April 2022, there was considerable potential aeolian transport (see maximum dune growth in Fig. 9A), exerting a negative impact on vegetation growth, evidenced by a below 5% simulated vegetation density towards April 2022. The results show that after April 2022, measured dune volume closely aligns with the maximum dune growth trend again, suggesting that vegetation is growing and surpassing 5% density, thereby capable of trapping aeolian sediment from the beach.

Two calibrated models effectively represent dune volume changes (Fig. 9A), demonstrating high accuracy with an r^2-value of 0.992 and an RMSE of 0.68 m^3/m. However, both exhibit distinct vegetation growth responses (Fig. 9C), with the most significant differences observed in the third year. It is important to note that while a calibrated model may closely reflect measured dune volume, this does not necessarily ensure realistic profile development (see section 3.4). To closely align with observed changes in dune volume and profile development, adjustments are made to the vegetation growth response beginning in the second year (see section 2.3). This involves modifying the vertical growth rate (V_{ver}) within the range of 0–2.5 m/year, typically with higher values during the growing season and periods of above-average precipitation, and increasing the maximum vegetation height ($h_{veg,max}$) from 1 to 2.2 m (see Fig. 5). While acknowledging that these values are unphysical, they provide a descriptive representation of vegetation density

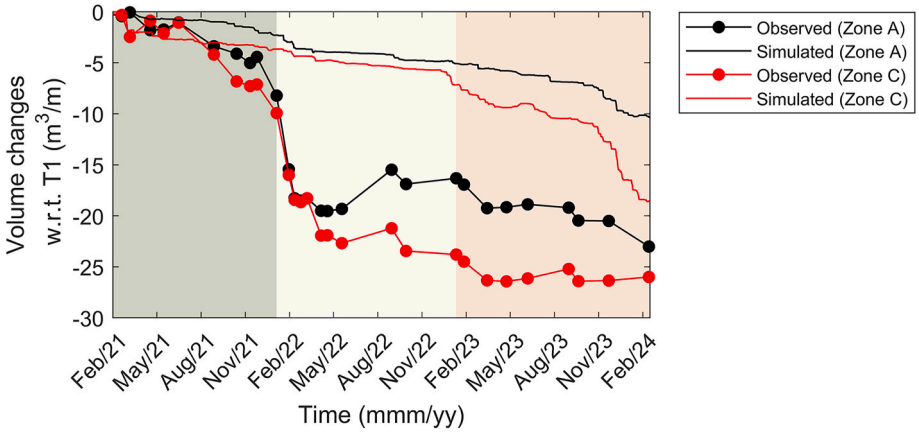

Fig. 8. Simulated net volume change of erosion volumes of the beach area compared to measured net volume change as presented in Strypsteen et al. (2024a). The background colours represent the three years.

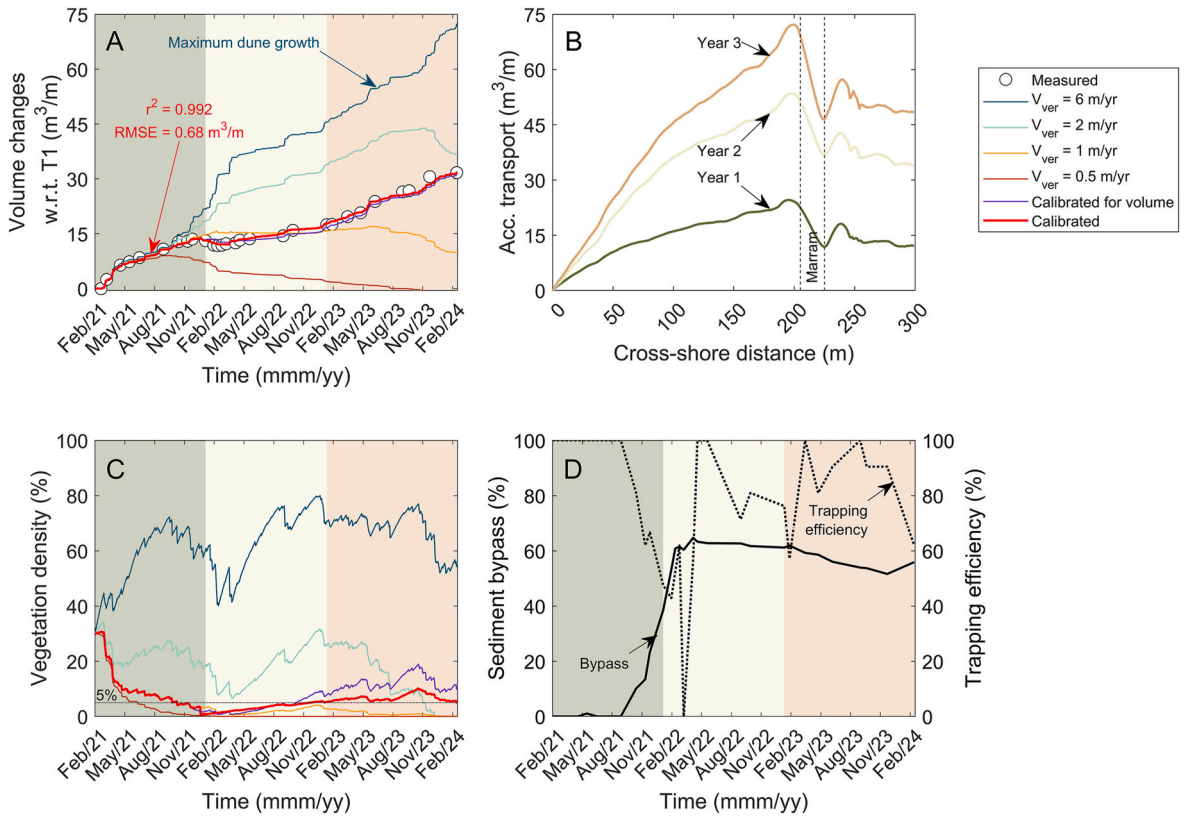

Fig. 9. A) Simulated net dune volume changes for different vegetation growth responses (ρ_{veg}), is compared against the measured net dune volume change, as presented in Strypsteen et al. (2024a). B) Variability in simulated accumulated transport rate along the cross-shore direction every consecutive year. C) Temporal variability in vegetation growth responses, and D) Temporal variability in sand trapping efficiency and sediment bypass of the vegetation for the calibrated model. The background colours represent the three years.

development in the calibrated models. The model calibrated for dune volume change maintains a consistent maximum vegetation height of 1 m throughout the entire timeframe, albeit with varying vertical growth rates.

In the calibrated models, vegetation density initially decreases in the first year, followed by a gradual increase in the second year and a more pronounced increase in the third year, concluding with a decrease in the last five months. The decrease in measured dune volume on January 31, 2022, was attributed to storm Corrie, resulting in minor dune toe erosion. While dune erosion caused by hydrodynamic processes is not simulated, the reduction in simulated dune volume is influenced by wind erosion combined with low vegetation density.

Sediment bypass, calculated by comparing accumulated sediment transport (Fig. 9B) to calibrated dune volume changes (Fig. 9A), quantifies sediment passing through the dune area. Fig. 9D indicates that approximately 55%–60% of sand bypassed the dune area over the three years. Trapping efficiency, defined as the ratio of sediment trapped by vegetation to the sediment input, varied over time, with 100% efficiency in the first nine months post-plantation, followed by seasonal variability in the subsequent years. During the months between November and March (winter period), when vegetation growth is slow, trapping efficiency decreased to 60% with higher bypass. Particularly between November 2021 and April 2022, trapping efficiency dropped to 0% due to already a very low vegetation density due to burial. However, during the vegetation growing season between April and October, trapping efficiency improved significantly, nearly reaching 100% reducing bypass. This is also conceptualized in Fig. 10.

3.3. Vegetation development for calibrated model

Fig. 11 shows the spatial variability of simulated vegetation development over time for the calibrated model. Initial vegetation densities diminished rapidly towards the end of the first year, a trend also noted by Strypsteen et al. (2024a). The simulated densities then increase again towards the end of the second and third year, followed by a subsequent decrease by the end of the third year. Generally, higher densities are simulated at the perimeters of the dune, which reflects observations by Strypsteen et al. (2024a). While these vegetation patterns seem to match observation, a closer evaluation shows a rather low spatial predictive power (Table 1).

The spatial organization of the vegetation density shows the best match - lowest Root Mean Squared Error (RMSE) and Mean Absolute Error (MAE) values - at the end of the first growing season (Year 1) when overall cover is low due to mass burial. Immediately after planting (Year 0), and after the second (Year 2) and third growing season (Year 3), deviations with observed values increase with the calibrated model systematically under-representing the observed values. The calibrated model consecutively predicts a larger spatial autocorrelation of the density relative to the one observed (Moran's I in Table 1). As described in Strypsteen et al. (2024a) the vegetation spatial pattern is evolving towards a random distribution in time, while model output conserves the initial spatial autocorrelation pattern.

3.4. Effect of vegetation growth rates on profile development

Fig. 12A–F illustrates the measured and simulated average profile development across the dune dimensions in both cross-shore and longshore directions over the course of three consecutive years. Measured topography changes are combined with the standard deviation indicating the spatial variability across dune width and length. The calibrated model demonstrates realistic profile developments closely aligned with measurements detailed in Strypsteen et al. (2024a),

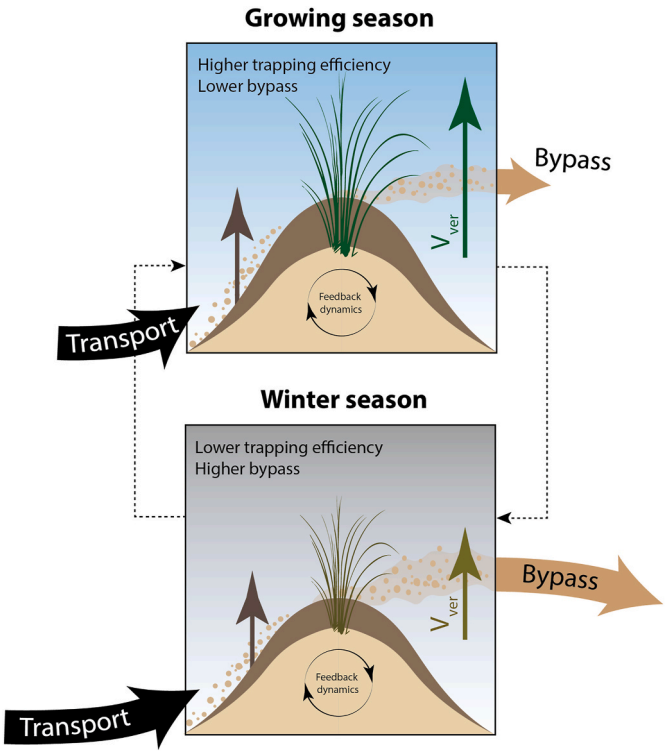

Fig. 10. Conceptual figure depicting the role of marram grass in dune formation across seasonal cycles. During the growing season, the robust growth of marram grass significantly increases the trapping efficiency and decreases sediment bypass. Conversely, in the winter season, reduced vegetative growth allows for increased sediment bypass and thus decreased trapping efficiency.

especially when compared to the model only calibrated for dune volume change. In the latter model, profile development undergoes a landward and northeastern shift due to different variations in vegetation behaviour calibrated with different vegetation values (Fig. 5), resulting in increased vegetation mortality in zones 1 to 3 compared to those shown in Fig. 11 (black areas).

It is evident that simulated erosion is largest in the cross-shore profiles between the landward boundary of the vegetation and the seawall. This phenomenon is attributed to the abrupt increase in wind shear velocity from the vegetated area to the bare sand surface (Strypsteen and de Vries, 2023). Additionally, less simulated erosion is observed in the adjacent beach areas where no vegetation is planted. Minor differences in cross- and longshore profile development are evident in the results of the end simulation. A slight landward shift and increased sediment accumulation in the centre of the dune occurs.

Compared to the calibrated simulation results, the model runs with higher vertical vegetation growth rates (>2 m/year) exhibit more pronounced profile development. It is evident that more sediment accumulates at the onshore and southwest boundaries, beyond the vegetation boundary, due to the spatial distribution of the shear stress. This aligns with the prevailing wind direction and stronger winds as illustrated in Fig. 4A, resulting in approximately 15% of the sand being deposited in these areas. Unlike the other vegetation growth responses examined in this study, the crest level of the maximum simulated dune would overpass the height of the seawall located at 9.4 m TAW. Time series of measured and modelled average dune crest level for the entire dune area is shown in Fig. 12G. The measurements are complemented with the standard deviation indicating the spatial variability across the dune area. The calibrated model results follow the temporal variability of the measurements very well with a r^2-value of 0.993 and RMSE of

Table 1
Comparison of vegetation density between calibrated model and observations for the consecutive years.

Comparison	RMSE density	MAE density	Moran's I (Simulated)	Moran's I (Observed)
Year 0	0.27	0.26	0.83	0.80
Year 1	0.05	0.04	0.85	0.46
Year 2	0.23	0.13	0.86	0.47
Year 3	0.37	0.26	0.88	0.54

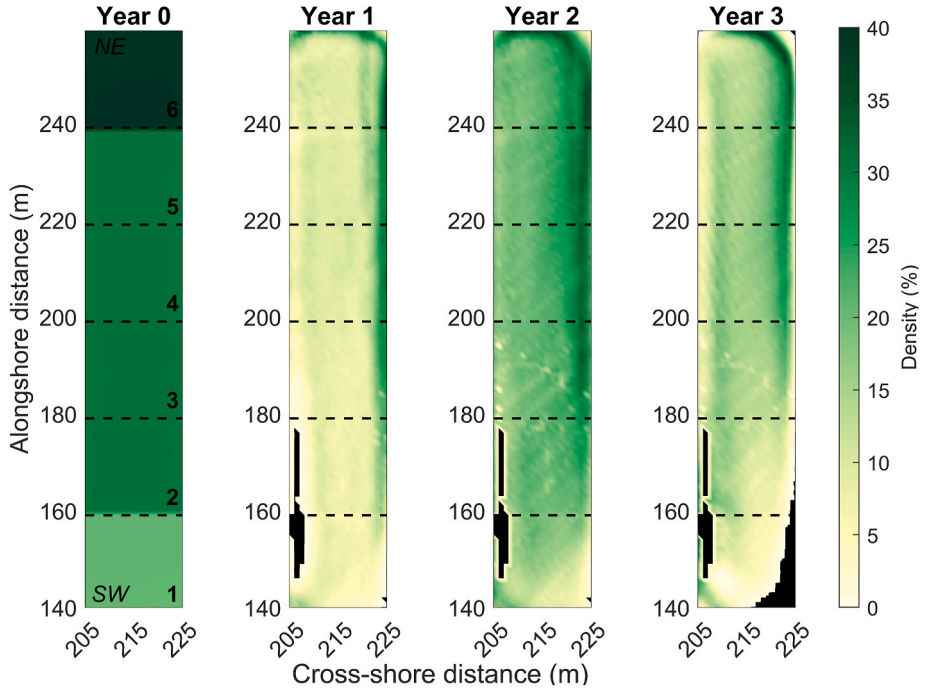

Fig. 11. Temporal and spatial simulated vegetation development across the initial six original planted zones. The areas where vegetation has died are indicated in black. The initial vegetation density in the simulations was 20%, 30%, and 40%.

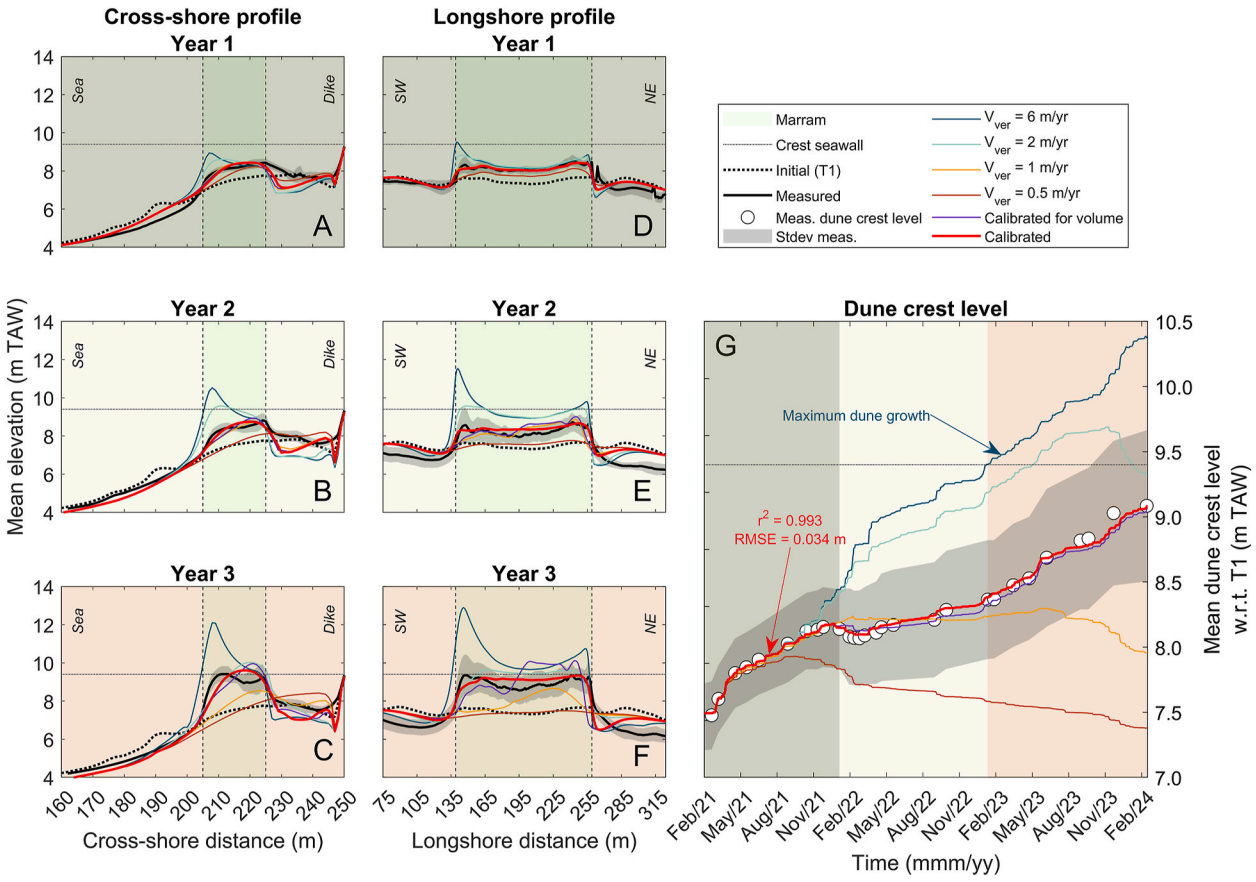

Fig. 12. A-F) The mean simulated profile development in both cross-shore and longshore directions is illustrated for various vegetation growth responses over the three-year period. The initial topography, measured during the T1 drone survey, is depicted as a reference for showcasing dune evolution by the dotted blue line. The corresponding measured topographies (T10, T20, and T28) are depicted by the black solid line, complemented with the standard deviation. The crest level of the seawall/dike is indicated by the dotted black line. Additionally, the boundaries of the planted marram grass are delineated by the dashed black lines, spanning 20 m in the cross-shore direction and 120 m in the longshore direction. Right panel: Simulated mean dune crest level above TAW for the different vegetation growth responses compared to measured mean dune height. Measured dune height is complemented with standard deviation. The background colours represent the three years.

0.034 m. In accordance with Fig. 9A, it is observed that the variability in average crest level correlates with the variability in dune volume change.

3.5. *Dune development for different dune widths*

As the calibrated model can reproduce dune volume changes, dune profile, and dune crest level reasonably well, it is possible to conduct a sensitivity analysis to understand how different dune constructions can affect dune evolution under the same vegetation growth response. After three years of wind forcing, Fig. 13 shows that for constructed dune widths ranging between 20 and 40 m, there is a corresponding increase in dune volume and a decrease in mean dune height as dune width increases. This is expected as more sediment from the beach can be deposited within the dune area because of aeolian transport. The cross-shore profile development appears to widen and flatten. In contrast, the longshore profile development appears to erode at the northeast boundary, leading to a decrease in mean dune height. Although the increase in dune volume with dune width is not linear, it appears to approach an asymptotic relationship.

4. Discussion

The AeoLiS model correctly reproduced multi-annual dune growth volumes. Dune toe erosion due to marine action was measured but was not simulated by the model. Maximum aeolian sand transport in the model, mirroring the findings of Strypsteen (2023), through the application of the van Rijn and Strypsteen (2020) transport equation, is well captured, especially when focusing on the initial nine months of dune evolution. Transport measurements conducted in these nine months during fetch effect measurements further validate the accurate computation of realistic maximum transport rates in the same study site (Strypsteen et al., 2024b).

The modelling results highlight the impact of various vegetation growth responses, indicating that dune evolution at the study site is largely driven by ecological processes. However, the currently assumed representation of ecological processes in AeoLiS simplifies vegetation growth and decay by focusing solely on fixed vertical vegetation growth rate that vary only with sediment burial. In reality, the establishment, growth, and resilience of dune vegetation are influenced by a multitude of biotic and abiotic factors, including salinity, wind stress, precipitation, groundwater levels, competition and lateral expansion, as well as removal by storm erosion (Homberger et al., 2024; Nield and Baas, 2008; Durán and Herrmann (2006a), (2006b); van Puijenbroek et al., 2017). Currently, the vertical vegetation growth rates are adjusted manually in the calibrated model, with only an implicit link to these factors. This aspect could be automated and expanded upon in future modelling efforts to include seasonal variability in vegetation growth. AeoLiS accommodates only one type of vegetation, yet multiple species with unique growth functions may be necessary for alternative landform simulations (Baas and Nield, 2007). Additionally, ongoing work involves coupling AeoLiS with DOONIES (Charbonneau et al., 2022), an

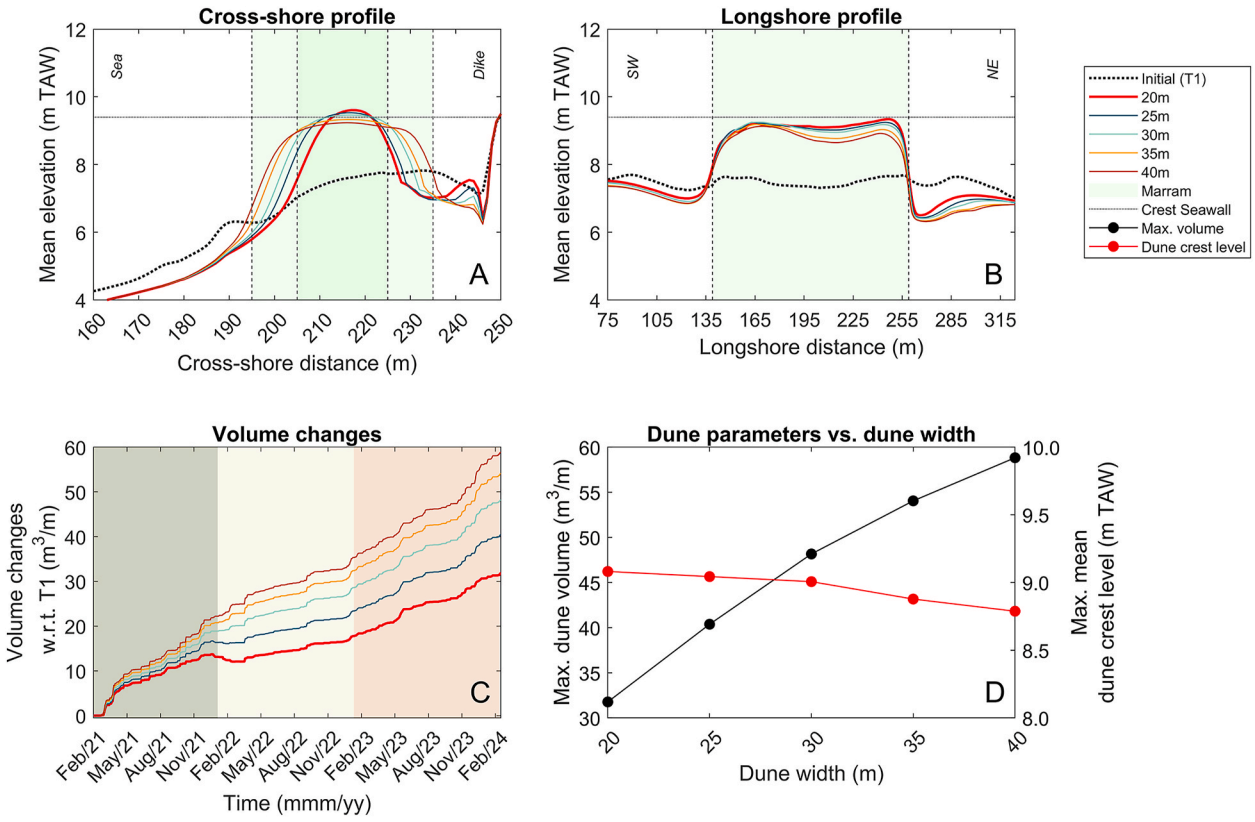

Fig. 13. Dune development is examined under various constructed dune widths ranging from 20 to 40 m. A-B) The cross- and longshore profile development is depicted, along with C) the timeseries of dune volume change and D) the relationship between dune width, maximum dune volume, and dune height. The background colours represent the three years.

ecological model based on photosynthesis developed for coastal environments, and with 'Living Dunes' (Bonte et al., 2021), which would add growth responses that vary with meteorological parameters and species differentiation.

Despite these complexities, the calibrated model effectively captures variations in dune volume by adjusting the vertical growth rate of vegetation. Notably, changes in the vertical growth rate show strong seasonal patterns and are associated with burial dynamics and meteorological variability (Bonte et al., 2021; Homberger et al., 2024; Nolet et al., 2018). The low match with the observed vegetation dynamics demonstrates, however, that this calibrated vegetation height and growth rate somehow captures changes in the spatial organization of the vegetation. The calibrated model for instance incorporated an increased vegetation growth rate toward the third year of dune evolution, while observed vegetation expansion rates remained consistent throughout the different growing seasons, averaging between 1.5 and 1.7 per year (Strypsteen et al., 2024a). The calibrated model systematically underestimated the spatial cover of the vegetation but overestimated the spatial clumpedness. The calibrated and exaggerated vegetation parameters were thus essential to mimic the needed shear stress reduction and subsequent dune volume evolution. A more mechanistic vegetation modelling approach, also incorporating temperature and humidity dependent growth processes, is needed to remove the aberrated parameterization while maintaining the physical aeolian coupling.

During the initial nine months post-plantation, the vegetation managed to cope up with the sediment input, as depicted in Fig. 9D, thus being 100% effective in trapping sand. The planted vegetation's rigidity, initial height, distribution, and density, combined with subsequent slow growth, likely facilitated effective sediment trapping. The high trapping efficiency of the vegetation in the model was achieved due to an initial high vegetation density. Despite the high dune growth rate in March and April 2021 (6 m^3/m), the simulated vegetation managed to keep up with the sediment input since the simulated vegetation density remained above 5%.

However, in the following months, vegetation did not keep pace with the sediment input, particularly when the simulated vegetation density fell below 5%. A density close to or below 5%, combined with high aeolian transport rates, appears to be detrimental to simulated dune growth and profile development, as demonstrated by the results in Fig. 9C, especially when compared to moderate transport rates over longer periods. From November 2021 to April 2022, a substantial potential aeolian transport of about 20 m^3/m was computed, indicating a considerable sediment influx into the dune. This sediment input affected vegetation growth, as burial rates exceeding the optimum can lead to a decline in vegetation growth (Nolet et al., 2018) (Fig. 2A).

Trapping efficiency during the observed dune evolution thus fluctuated over time, exhibiting seasonal variability (Fig. 9D). In the colder months from November to March, when vegetation growth is minimal (Huiskes, 1979), trapping efficiency decreased to 60%. Between November 2021 and April 2022, trapping efficiency even declined to 0%. Conversely, during the warmer growing season from April to October, trapping efficiency notably improved, nearly reaching 100%. This suggests that dune growth is influenced not only by the seasonal variation in wind speed but also by the seasonality of vegetation growth (van Puijenbroek et al., 2017). The fact that trapping efficiency was 100% during the initial nine months of dune evolution, even during the high transport events in March and April 2021, may indicate that vegetation density, affecting wind speed reduction as outlined by Raupach et al. (1993), was higher at the beginning of dune evolution than in the subsequent months and years of the study period. Sediment bypassing the dune is transported landward towards the seawall and along the shoreline.

Fig. 14 shows the observed evolution of vegetation growth at the study site over the three-year period, illustrating the initial plantation,

subsequent decline, and eventual increase in vegetation height throughout the years. Indeed, vegetation became more spread in thicker and higher bundles compared to the initial planting strategy with more bare sand patches. In September 2023, the simulated vegetation density was 1.5–3 times lower than that of the initial plantation, despite a notable change in the appearance of the vegetation (height and distribution) during this period. Strypsteen et al. (2024a) observed an overall increase in vegetation cover, which would indicate an increase in density over the three-year period. This scenario illustrates the "telephone pole problem" outlined by Okin (2008). While two surfaces exhibit identical vegetation density, one may feature numerous shorter vegetation bundles, while the other has fewer but taller bundles. Both surfaces would undergo the same wind shear reduction but different profile development, following the principles defined by Raupach et al. (1993).

Vegetation density alone, in combination with the Raupach et al. (1993) vegetation shear coupler, does not provide insights into vegetation distribution or the presence of bare sand patches within the dune system causing a more variable topography. The vegetation model of Okin (2008) can offer valuable insights into introducing spatial patterns into vegetation for 2D simulations, but the approach remains static.

Nevertheless, it is worth noting that the AeoLiS model effectively reproduces profile development in both cross-shore and alongshore directions. Notably, the final simulated profile closely mirrors the initial topography, particularly evident in the longshore direction. However, a slight dip in the dune cross- and longshore profile, attributed to local variations in vegetation growth or mortality, is observed in the measurements (Fig. 12A–F), persisting throughout the dune evolution. This nuanced feature may be indicative of complex biotic and abiotic interactions which are not fully captured by the model's vegetation module. Furthermore, the dune body shifted slightly landward in the model due to strong onshore winds early in the second year and persisted throughout the third year, a shift which is not observed in the measurements. Instead, observations showed a 1 m-high scarp formed at the dune toe due to storm erosion during storm Corrie (Strypsteen et al., 2024a), a feature not captured in the model. Consequently, measured sand deposited after storm Corrie accumulated largely at the dune toe. This scarp feature may have prevented the dune from shifting landward.

Surface moisture and sediment texture variability can introduce supply limitations that affect expected transport rates under specific wind conditions and alter critical fetch distances (Strypsteen et al., 2024b). Although not included in this study, investigating the effects of surface moisture on dune evolution presents an intriguing avenue for future research.

Topographic steering of wind in AeoLiS is simulated using shear stress perturbations as described by Weng et al. (1991). However, the presence of steep slopes, which are common in coastal areas, limits the applicability of this theory. The current AeoLiS code cannot describe complex flow structures around steep topographic gradients or flow reversal on the lee side of dunes, which impacts aeolian transport predictions. However, steep slopes are often coupled with vegetated surfaces. Field observations indicate that the influence of vegetation roughness outweighs the effects of topographic steering van Westen et al. (2024a). Although shear stress may increase across a steep foredune, aeolian transport remains negligible due to the presence of vegetation.

4.1. Local management implications

For the current modelled dune width of 20 m, an increase in vegetation density is anticipated to result in an overall larger net accretion. This aligns with field observations indicating that higher vegetation densities allow for increased sand accumulation in the dune, provided there is sufficient sand availability (Derijckere et al., 2023; Hesp et al., 2019; Shumack et al., 2022). However, achieving these higher densities necessitates unrealistic vegetation growth rates since normal growth rates vary between 0 and 1 m/year (Nolet et al., 2018), suggesting that

Fig. 14. Vegetation development from the initial plantation to three years later (© Photographs by Glenn Strypsteen).

the maximum dune size would not have been reached with a width of 20 m alone. Conversely, when utilizing the calibrated model for wider dunes up to 40 m, it is evident that a larger dune width leads to a greater dune volume. This underscores the importance of dune width in trapping larger sediment volumes. However, while dune width influences sediment trapping, it does not necessarily correspond to increased mean dune height, as observed in this study. These findings collectively suggest that planting strategies could be optimized to promote dune widening by initially establishing wider dune plantations which is helpful for reducing storm impact on the hinterland. However, the interaction between a larger seaward dune field and the seawall will likely introduce complex wind fields beyond the scope of Weng et al. (1991)'s theory, which cannot be described by AeoLiS (van Westen et al., 2024a). However, these simulation results may not be directly transferable to other sites, as dune development is influenced by a range of factors, including sand availability, beach characteristics, grain size, and other local conditions.

5. Conclusions

This study aimed to use the AeoLiS model to simulate the three-year ecological and morphological characteristics of a marram grass planted dune pilot site in Oosteroever, Belgium. We pursued three specific objectives: (1) evaluate dune evolution under varying ecological growth conditions, (2) calibrate AeoLiS using high-resolution field data, and (3) conduct a sensitivity analysis on different dune widths. The answers to these objectives are summarized below.

1. Our simulations revealed that vegetation dynamics, particularly marram grass growth, are crucial for dune evolution. Seasonal variations in vegetation, driven by sediment burial, precipitation, and growing season, substantially affect sediment trapping efficiency. This underscores the need to consider ecological dynamics when assessing dune evolution.
2. AeoLiS was successfully calibrated with high-resolution data, accurately reflecting sediment deposition, vegetation response, and profile changes over three years. While the model effectively simulated key processes, some discrepancies in profile development highlighted limitations in capturing all influencing factors, pointing to areas for model refinement. The exclusion of biotic and abiotic factors influencing vegetation dynamics, underscores the complexity inherent in coastal eco-geomorphological processes.
3. The sensitivity analysis showed that wider dunes at the study site improve sediment trapping efficiency without significantly increasing dune height. This suggests that optimizing dune width can enhance sediment capture and inform coastal management practices.

The findings advocate for further research to refine dune modelling and explore planting strategies to increase coastal resilience.

CRediT authorship contribution statement

Glenn Strypsteen: Writing – review & editing, Writing – original draft, Visualization, Validation, Software, Resources, Project administration, Methodology, Investigation, Funding acquisition, Formal analysis, Data curation, Conceptualization. **Sierd de Vries:** Writing – review & editing, Software. **Bart van Westen:** Writing – review & editing, Software. **Dries Bonte:** Writing – review & editing. **Jan-Markus Homberger:** Writing – review & editing. **Caroline Hallin:** Writing – review & editing. **Pieter Rauwoens:** Writing – review & editing, Supervision.

Declaration of competing interest

The authors declare that they have no known competing financial interests or personal relationships that could have appeared to influence the work reported in this paper.

Data availability

Data will be made available on request.

Acknowledgements

We thank the invaluable contributions of Sam Provoost, Toon Verwaest, Steven Muylaert, Wim van Calster, and Peter van Besien to the 'dune-in-front-of-a-dike' project. Frederik Vandaele provided the vegetation comparisons between the AeoLiS simulations and measured values. This study was made possible through funding from the Research Foundation - Flanders (Fonds Wetenschappelijk Onderzoek, number 1243022N), as well as support from the Flemish Government, Department of Mobility and Public Works, for the use of the drone data. Part of this research has also received funding from the European Union's Horizon Europe research and innovation programme under grant agreement No 101135410 – The DuneFront Project. Field data collection received invaluable assistance from several individuals, including Bart Roest, Jennifer Derijckere, Jadon Beerlandt, and several master's students. And lastly, thanks to Íngrid Amer Cid for the valuable discussions.

Appendix A. Model settings

Parameter	Value	Description
Timing		
dt	7 200 s	Time interval between timesteps
tstart	2 761 200 s	Starting time of the simulation (February 12, 2021 00:30)
tstop	99 813 600 s	End time of the simulation (March 11, 2024 07:30)
output_times	86 400 s	Time interval between *.nc output file
Processes (only enabled processes)		
process_shear	True	Enable the process of wind shear
process_wind	True	Enable the process of wind
process_tide	True	Enable the process of tides
process_wave	True	Enable the process of waves
process_runup	True	Enable the process of wave runup
process_threshold	True	Enable the process of threshold
process_transport	True	Enable the process of transport
process_bedupdate	True	Enable the process of bed updating
process_separation	True	Enable the including of separation bubble
process_nelayer	True	Enable a non-erodible layer

(*continued on next page*)

(*continued*)

Parameter	Value	Description
process_vegetation	True	Enable the process of vegetation
Threshold		
th_grainsize	True	Enable wind velocity threshold based on grainsize
th_bedslope	True	Enable wind velocity threshold based on bed slope
th_nelayer	True	Enable wind velocity threshold based on a non-erodible layer
General physics		
g	9.81 m/s^2	Gravitational constant
v	0.000015 m^2/s	Air viscosity
rhoa	1.225 kg/m^3	Air density
rhog	2 650.0 kg/m^3	Grain density
rhow	1 025.0 kg/m^3	Water density
porosity	0.4	Sediment porosity
cpair	0.0010035 MJ/kg/°C	Specific heat capacity air
Sediment		
nlayers	1	Number of bed layers
layer_thickness	0.05 m	Thickness of bed layers
nfractions	1	Number of sediment fractions
grain_dist	1	Initial distribution of sediment fractions
grain_size	0.00025 m	Average grain size of each sediment fraction
Wind and shear		
wind_convention	nautical	Convention used for the wind direction in the input files (cartesian or nautical)
alfa	60 deg	Real-world grid cell orientation with respect to the North (clockwise)
z	10 m	Measurement height of wind velocity
kappa	0.4	Von Kármán constant
L	100 m	Typical length scale of dune feature (perturbation)
l	10 m	Inner layer height (perturbation)
m	0.5	Factor to account for difference between average and maximum shear stress
Sediment transport		
bi	0.5	Bed interaction factor
method_transport	vanrijn_strypsteen	Name of method to compute equilibrium sediment transport rate
method_roughness	vanrijn_strypsteen	Name of method to compute roughness
Aa	0.1	Constant in formulation for wind velocity threshold based on grain size
Cb	1.5	Constant in Bagnold formulation for equilibrium sediment concentration
method_grainspeed	windspeed	Name of method to assume/compute grain speed
Solver		
T	1 s	Adaptation time scale in advection equation
solver	steadystate	Numerical solver of advection scheme
CFL	1	CFL number to determine time step in explicit scheme
accfac	1	Numerical acceleration factor
scheme	euler_backward	Name of numerical scheme
max_error	0.000001	Maximum error at which to quit iterative solution in implicit numerical schemes
max_iter	1 000	Maximum number of iterations at which to quit iterative solution in implicit numerical schemes
Boundary conditions		
boundary_onshore	constant	Name of onshore boundary conditions
boundary_lateral	circular	Name of lateral boundary conditions
boundary_offshore	constant	Name of offshore boundary conditions
Vegetation		
gamma_vegshear	16	Roughness factor for the shear stress reduction by vegetation
avg_time	86 400 s	Indication of the time period over which the bed level change is averaged for vegetation growth
dzb_interval	86 400 s	Interval used for calculation of vegetation growth
hveg_max	1 m and 2.2 m	Max height of vegetation
dzb_opt	0.31 m/year	Sediment burial for optimal growth
V_ver	0–2 m/year	Vertical growth
V_lat	0 m/year	Lateral growth
germinate	0/year	Possibility of germination per year
Lateral	0/year	Possibility of lateral expansion per year
veg_gamma	1	Constant on influence of sediment burial
veg_sigma	2	Sigma in gaussian distribution of vegetation cover filter
vegshear_type	Raupach	Vegetation shear solver
Separation		
c_b	0.2	Slope at the leeside of the separation bubble
mu_b	20 deg	Minimum required slope for the start of flow separation
Waves		
Tswash	30 s	Adaptation time for resetting morphology in the Swash-zone
xi	0.3	Surf similarity parameter
facDOD	0.1	Ratio between depth of disturbance and local wave height

References

Baas, A.C.W., Nield, J.M., 2007. Modelling vegetated dune landscapes. Geophys. Res. Lett. 34 (6). https://doi.org/10.1029/2006GL029152.

Bagnold, R.A., 1954. The Physics of Blown Sand and Desert Dunes, second ed. Methuen, London.

Bauer, B.O., Davidson-Arnott, R.G.D., 2003. A general framework for modeling sediment supply to coastal dunes including wind angle, beach geometry, and fetch effects. Geomorphology 49 (1), 89–108. https://doi.org/10.1016/S0169-555X(02)00165-4.

Bonte, D., Batsleer, F., Provoost, S., Reijers, V., Vandegehuchte, M.L., Van De Walle, R., Dan, S., Matheve, H., Rauwoens, P., Strypsteen, G., Suzuki, T., Verwaest, T., Hillaert, J., 2021. Biomorphogenic feedbacks and the spatial organization of a dominant grass steer dune development. Frontiers in Ecology and Evolution 9 (October), 1–12. https://doi.org/10.3389/fevo.2021.761336.

Bonte, D., Consortium, D., 2024. Designing dunes in front of dikes: a hybrid blue-grey solutions for coastal safety under climate change. EGU General Assembly 2024. https://doi.org/10.5194/egusphere-egu24-10562. Vienna, Austria, 14-19 Apr 2024, EGU24-10562.

Charbonneau, B.R., Duarte, A., Swannack, T.M., Johnson, B.D., Piercy, C.D., 2022. DOONIES: a process-based ecogeomorphological functional community model for coastal dune vegetation and landscape dynamics. Geomorphology 398, 108037. https://doi.org/10.1016/j.geomorph.2021.108037.

Cohn, N., Hoonhout, B.M., Goldstein, E.B., Vries, S. De, 2019. Exploring marine and aeolian controls on coastal foredune growth using a coupled numerical model, 1–25. https://doi.org/10.3390/jmse7010013.

Danin, A., 1991. Plant adaptations in desert dunes. J. Arid Environ. 21 (2), 193–212. https://doi.org/10.1016/s0140-1963(18)30682-7.

Dauwe, S., Verleye, T., Devriese, L., Belpaeme, K., Maelfait, H., Pirlet, H., Mees, J., 2019. Het KustINzicht 2019 - Compendium voor Kust en Zee. Vlaams Instituut voor de Zee (VLIZ), p. 193. https://www.vliz.be/imisdocs/publications/339408.pdf.

de Vries, S., Hallin, C., van Ijzendoorn, C., van Westen, B., Cohn, N., Strypsteen, G., Skaden, J., Agrawal, N., Garcia Alvarez, M., 2023. AeoLiS (v3.0.0rc2). Zenodo. https://doi.org/10.5281/zenodo.10071595.

de Winter, R.C., Gongriep, F., Ruessink, B.G., 2015. Observations and modeling of alongshore variability in dune erosion at Egmond aan Zee, The Netherlands. Coast Eng. 99, 167–175. https://doi.org/10.1016/j.coastaleng.2015.02.005.

Delgado-Fernandez, I., Davidson-Arnott, R., 2011. Meso-scale aeolian sediment input to coastal dunes: the nature of aeolian transport events. Geomorphology 126 (1–2), 217–232. https://doi.org/10.1016/j.geomorph.2010.11.005.

Derijckere, J., 2021. Monitoring en modellering van duinvorming bij nieuwe aanplant (MSc. dissertation). KU Leuven, Bruges, Belgium.

Derijckere, J., Strypsteen, G., Rauwoens, P., 2023. Early-stage development of an artificial dune with varying plant density and distribution. Geomorphology 437 (January), 108806. https://doi.org/10.1016/j.geomorph.2023.108806.

Dickey, J., Wengrove, M., Cohn, N., Ruggiero, P., Hacker, S.D., 2023. Observations and modeling of shear stress reduction and sediment flux within sparse dune grass canopies on managed coastal dunes. Earth Surf. Process. Landforms 48 (5), 907–922. https://doi.org/10.1002/esp.5526.

Durán, O., Herrmann, H., 2006a. Modelling of saturated sand flux. J. Stat. Mech. Theor. Exp. 7. https://doi.org/10.1088/1742-5468/2006/07/P07011.

Durán, O., Herrmann, H.J., 2006b. Vegetation against dune mobility. Phys. Rev. Lett. 97 (18), 1–4. https://doi.org/10.1103/PhysRevLett.97.188001.

Durán, O., Moore, L.J., 2013. Vegetation controls on the maximum size of coastal dunes. Proc. Natl. Acad. Sci. USA 110 (43), 17217–17222. https://doi.org/10.1073/pnas.1307580110.

Elko, N., Brodie, K., Stockdon, H., Nordstrom, K., Houser, C., McKenna, K., Moore, L., Rosati, J., Ruggiero, P., Thuman, R., Walker, I., 2016. Dune management challenges on developed coasts. Shore Beach 84 (1), 15.

Haerens, P., Bolle, A., Trouw, K., Houthuys, R., 2012. Definition of storm thresholds for significant morphological change of the sandy beaches along the Belgian coastline. Geomorphology 143–144, 104–117. https://doi.org/10.1016/j.geomorph.2011.09.015.

Hallin, C., Ijzendoorn, C. van, Homberger, J.M., de Vries, S., 2023. Simulating surface soil moisture on sandy beaches. Coast Eng. 185 (June), 104376. https://doi.org/10.1016/j.coastaleng.2023.104376.

Heminway, S.S., Cohn, N., Davis, E.H., White, A., Hein, C.J., Zinnert, J.C., 2024. Exploring ecological , morphological , and environmental controls on coastal foredune evolution at annual scales using a process-based model. Sustainability 16 (3460), 1–23. https://doi.org/10.3390/su16083460.

Hesp, P.A., 1988. Surfzone, beach, and foredune interactions on the Australian South East coast. J. Coast Res. 3, 15–25.

Hesp, P.A., 1991. Ecological processes and plant adaptations on coastal dunes. In: Journal of Arid Environments, 21, pp. 165–191. https://doi.org/10.1016/s0140-1963(18)30681-5, 2.

Hesp, P.A., 2002. Foredunes and blowouts: initiation, geomorphology and dynamics. Geomorphology 48 (1–3), 245–268.

Hesp, P.A., Dong, Y., Cheng, H., Booth, J.L., 2019. Wind flow and sedimentation in artificial vegetation: field and wind tunnel experiments. Geomorphology 337, 165–182. https://doi.org/10.1016/j.geomorph.2019.03.020.

Homberger, J., Lynch, A., Riksen, M., Limpens, J., 2024. Growth response of dune-building grasses to precipitation. Ecohydrology e2634 (October 2023), 1–16. https://doi.org/10.1002/eco.2634.

Hoonhout, B., de Vries, S., 2016. A process-based model for aeolian sediment transport and spatiotemporal varying sediment availability. J. Geophys. Res.: Earth Surf. 121 (8), 1555–1575. https://doi.org/10.1002/2015JF003692.

Hoonhout, B., de Vries, S., 2019. Simulating spatiotemporal aeolian sediment supply at a mega nourishment. Coast Eng. 145 (March 2018), 21–35. https://doi.org/10.1016/j.coastaleng.2018.12.007.

Huiskes, A.H.L., 1979. Ammophila Arenaria (L .) Link (Psamma Arenaria (L .) Roem . et Schult .; Calamgrostis Arenaria (L .) Roth). J. Ecol. 67 (1), 363–382.

Keijsers, J.G.S., de Groot, A.V., Riksen, M.J.P.M., 2016. Modeling the biogeomorphic evolution of coastal dunesin response to climate change. J. Geophys. Res.: Earth Surf. 121, 1161–1181. https://doi.org/10.1002/2015JF003815. Received.

Keijsers, J.G.S., De Groot, A.V., Riksen, M.J.P.M., 2015. Vegetation and sedimentation on coastal foredunes. Geomorphology 228, 723–734. https://doi.org/10.1016/j.geomorph.2014.10.027.

Lomborg, B., 2020. False Alarm: How Climate Change Panic Costs Us Trillions, Hurts the Poor, and Fails to Fix the Planet. Basic Books.

Marshall, J.K., 1971. Drag measurements in roughness arrays of varying density and distribution. Agric. Meteorol. 8 (C), 269–292. https://doi.org/10.1016/0002-1571(71)90116-6.

Matias, A., Ferreira, O., Mendes, I., Dias, J.A., Vila-Concejo, A., 2005. Artificial construction of dunes in the south of Portugal. J. Coast Res. 213, 472–481.

Maun, M.A., 1998. Adaptations of plants to burial in coastal sand dunes. Can. J. Bot. 76 (5), 713–738. https://doi.org/10.1139/cjb-76-5-713.

Montreuil, A.-L., Elyahyioui, J., Chen, M., 2016. Effect of large-scale atmospheric circulation and wind on storm surge occurrence. Proceedings of the 14th International Coastal Symposium 75, 755.

Nield, J.M., Baas, A.C.W., 2008. The influence of different environmental and climatic conditions on vegetated aeolian dune landscape development and response. Global Planet. Change 64 (1–2), 76–92. https://doi.org/10.1016/j.gloplacha.2008.10.002.

Nolet, C., van Puijenbroek, M., Suomalainen, J., Limpens, J., Riksen, M., 2018. UAV-imaging to model growth response of marram grass to sand burial: implications for coastal dune development. Aeolian Research 31 (March 2017), 50–61. https://doi.org/10.1016/j.aeolia.2017.08.006.

Okin, G.S., 2008. A new model of wind erosion in the presence of vegetation. J. Geophys. Res.: Earth Surf. 113 (2), 1–11. https://doi.org/10.1029/2007JF000758.

Psuty, N.P., 2004. The coastal foredune : a morphological basis for regional coastal dune development. Ecol. Stud. 171, 11–27.

Raupach, M.R., 1992. Drag and drag partition on rough surfaces. Boundary-Layer Meteorol. 60 (4), 375–395.

Raupach, M.R., Gillette, D.A., Leys, J.F., 1993. The effect of roughness elements on wind erosion threshold. J. Geophys. Res. 98 (D2), 3023–3029. https://doi.org/10.1029/92JD01922.

Short, A.D., Hesp, P.A., 1982. Wave, beach and dune interactions in southeastern Australia. Mar. Geol. 48 (3–4), 259–284.

Shumack, S., Farebrother, W., Hesse, P., 2022. Quantifying vegetation and its effect on aeolian sediment transport: a UAS investigation on longitudinal dunes. Aeolian Research 54 (December 2021), 100768. https://doi.org/10.1016/j.aeolia.2021.100768.

Stive, M.J.F., de Schipper, M.A., Luijendijk, A.P., Aarninkhof, S.G.J., van Gelder-Maas, C., van Thiel de Vries, J.S.M., de Vries, S., Henriquez, M., Marx, S., Ranasinghe, R., 2013. A new alternative to saving our beaches from sea-level rise: the sand engine. J. Coast Res. 290, 1001–1008. https://doi.org/10.2112/JCOASTRES-D-13-00070.1.

Strypsteen, G., 2019. Monitoring and Modeling Aeolian Sand Transport at the Belgian Coast (PhD Thesis). KU Leuven, Bruges, Belgium.

Strypsteen, G., 2023. The importance of grain-related shear velocity in predicting multi-monthly dune growth. Earth Surf. Process. Landforms 48 (15), 3287–3301. https://doi.org/10.1002/esp.5696.

Strypsteen, G., Bonte, D., Taelman, C., Derijckere, J., Rauwoens, P., 2024a. Three years of morphological dune development after planting marram grass on a beach. Earth Surf. Process. Landforms. https://doi.org/10.1002/esp.5870.

Strypsteen, G., de Vries, S., 2023. Simulating profile development of new artifical dune with planted vegetation for sand nuisance mitigation. Proceedings of the Coastal Sediments 2023, pp. 732–738. *New Orleans, LA, 11–15 April 2023*.

Strypsteen, G., Delgado-Fernandez, I., Derijckere, J., Rauwoens, P., 2024b. Fetch-driven aeolian sediment transport on a sandy beach: a new study. Earth Surf. Process. Landforms 1–14. https://doi.org/10.1002/esp.5784. January.

Strypsteen, G., Houthuys, R., Rauwoens, P., 2019. Dune volume changes at decadal timescales and its relation with potential aeolian transport. J. Mar. Sci. Eng. 7 (10). https://doi.org/10.3390/jmse7100357.

Tresca, A., Ruz, M.H., Grégoire, P., 2014. Coastal dune development and sand drifting management along an artificial shoreline: the case of Dunkirk harbour, northern France. J. Coast Conserv. 18 (5), 495–504. https://doi.org/10.1007/s11852-013-0302-z.

van IJzendoorn, C.O., Hallin, C., Reniers, A.J.H.M., de Vries, S., 2023. Modeling multi-fraction coastal aeolian sediment transport with horizontal and vertical grain-size variability. J. Geophys. Res.: Earth Surf. 128 (7). https://doi.org/10.1029/2023JF007155.

van Puijenbroek, M.E.B., Limpens, J., de Groot, A.V., Riksen, M.J.P.M., Gleichman, M., Slim, P.A., van Dobben, H.F., Berendse, F., 2017. Embryo dune development drivers: beach morphology, growing season precipitation, and storms. Earth Surf. Process. Landforms 42 (11), 1733–1744. https://doi.org/10.1002/esp.4144.

van Rijn, L.C., Strypsteen, G., 2020. A fully predictive model for aeolian sand transport. Coast Eng. 156. https://doi.org/10.1016/j.coastaleng.2019.103600.

van Westen, B., de Vries, S., Cohn, N., van Ijzendoorn, C., Strypsteen, G., Hallin, C., 2024a. AeoLiS : numerical modelling of coastal dunes and aeolian landform development for real-world applications. Environ. Model. Software 179 (June), 1–19. https://doi.org/10.1016/j.envsoft.2024.106093Received.

van Westen, B., de Vries, S., Reniers, A.J.H.M., den Bieman, J.P., Hoonhout, B.M., Rauwoens, P., van Puijenbroek, M.E.B., 2019. Aeolian modelling of coastal landform development. Proceedings of the Coastal Sediments 2019, pp. 1354–1364.

van Westen, B., Luijendijk, A.P., de Vries, S., Cohn, N., Leijnse, T.W.B., de Schipper, M. A., 2024b. Predicting marine and aeolian contributions to the Sand Engine's evolution using coupled modelling. Coast Eng. 188 (January 2024). https://doi.org/10.1016/j.coastaleng.2023.104444.

Vousdoukas, M.I., Mentaschi, L., Voukouvalas, E., Verlaan, M., Feyen, L., 2017. Extreme sea levels on the rise along Europe's coasts. Earth's Future 5 (3), 304–323. https://doi.org/10.1002/2016EF000505.

Wang, H., Liu, X., Zhao, C., Chang, Y., Liu, Y., Zang, F., 2021. Spatial-temporal pattern analysis of landscape ecological risk assessment based on land use/land cover change in Baishuijiang National nature reserve in Gansu Province, China. Ecol. Indicat. 124, 107454. https://doi.org/10.1016/j.ecolind.2021.107454.

Weng, W., Hunt, J., Carruthers, D., Warren, A., Wiggs, G., Livingstone, I., Castro, I., 1991. Air flow and sand transport over sand-dunes. In: Aeolian Grain Transport: the Erosional Environment. Springer.

Wolfe, S.A., Nickling, W.G., 1993. The protective role of sparse vegetation in wind erosion. Prog. Phys. Geogr. 17 (1), 50–68. https://doi.org/10.1177/030913339301700104.